

Hidden Thresholds: A Technique for Reconstructing New Physics Masses at Hadron Colliders

P. Huang, N. Kersting¹, H.H. Yang

Physics Department, Sichuan University (Chengdu), P.R. China 610065

Abstract

We present an improved method of reconstructing New Physics (NP) masses from invariant mass endpoints. While the traditional method focuses on a single NP decay, our method considers the decays of two or more NP particles ($ABC\dots$) in a grander decay chain: $\textit{anything} \rightarrow ABC\dots \rightarrow \dots \rightarrow \textit{jets} + \textit{leptons}$. Though the center-of-mass energy E_{CM} of ‘anything’ varies unpredictably at a hadron collider, a sample of many events nonetheless expresses features of threshold production $E_{CM} = m_A + m_B + \dots$: invariant masses constructed from the final jet and lepton momenta are correlated in a way that makes their threshold endpoints visually obvious in a scatterplot. We illustrate this technique for the production of two neutralinos in the MSSM: $\textit{anything} \rightarrow \tilde{\chi}_i^0 \tilde{\chi}_j^0$ ($i, j = 2, 3, 4$) which subsequently decay via on- or off-shell sleptons to four leptons. Assuming the relevant SUSY spectrum is below 1 TeV and squarks/gluinos eventually decay to neutralinos, our MC study shows that one low-luminosity year at the LHC ($10 - 30 fb^{-1}$) can quantitatively determine on- versus off-shell decays and find the relevant neutralino and slepton masses to less than 10 percent.

¹Email: nkersting@scu.edu.cn

1 Introduction

At a hadron collider such as the Tevatron at Fermilab or the Large Hadron Collider (LHC) at CERN, searches for New Physics (NP) states beyond the Standard Model (SM) must take into account the fact that partonic center of mass energies at these machines are not tunable (as they will be at a much anticipated e^+e^- linear collider [1]) but vary continuously in principle from zero to the combined hadronic energies of approximately 2 TeV and 14 TeV, respectively. Moreover, many NP models predict the production of a long-lived particle that is likely to escape the detectors, carrying away missing energy. The traditional method of seeing a NP mass as a sharp resonance in a cross section is therefore not applicable, and we must consider other approaches to precision measurement of NP masses crucial for testing properties of an underlying fundamental theory.

One well-studied avenue is to construct invariant mass distributions of final jet or leptonic momenta in exclusive channels and study their endpoints. Even if some NP particles carry away missing energy in each event, endpoints of said distributions can be measured and matched to analytical functions of NP masses [2]. There are several caveats to this method however. First, the exclusive channel under study must somehow be identified or assumed. Second, backgrounds must not interfere with endpoint measurement. Third, there may be some model-dependence in the method of fitting the endpoint on a 1-dimensional histogram. The first caveat is the most difficult to deal with, especially in a model such as the Minimal Supersymmetric SM (MSSM), where the gluino and squarks decay via literally hundreds of possible decay chains ("cascades"). Studies of cascades which have enough endpoints to solve for MSSM masses, e.g. $\tilde{g} \rightarrow \tilde{q}q \rightarrow \tilde{\chi}_2^0 qq \rightarrow \tilde{l}^\pm l^\mp qq \rightarrow l^\pm l^\mp qq \tilde{\chi}_1^0$, usually just focus on a few 'benchmark scenarios' [3, 4] which, however, may not be what Nature chooses. As for eliminating SM backgrounds, requiring a suitable number of hard jets and isolated leptons may suffice; NP backgrounds are more challenging and, if these can be reduced, typically also inflict damage in the region of the desired endpoint where rates are already low². This then brings up the third problem of how to fit the endpoint. Linear or Gaussian fits are most convenient, but very detailed study of cuts and detector effects are required to understand their general accuracy [5].

In this work we wish to show that there are two important features of NP particle production which, when used together, can greatly boost the efficacy of the endpoint method. First, if NP particles carry a new conserved charge, such as R-parity in the MSSM, they will be multiply-produced. We may, for example, consider inclusive decay chains of the form $\mathbb{X} \rightarrow AB \rightarrow \text{jets} + \text{leptons}$, where A and B are NP states and \mathbb{X} is any system of particles with a sufficiently large total invariant mass: $m_{\mathbb{X}} \geq m_A + m_B$ (the case where $m_{\mathbb{X}} = m_A + m_B$ is especially important and we designate this 'threshold production.'). Since \mathbb{X} usually includes at least one multi-particle system, $m_{\mathbb{X}}$ really is continuously-valued from the threshold value all the way up to the machine energy. Second, depending on $m_{\mathbb{X}}$ and the exact way in which AB

²One notable exception is the decay $A \rightarrow B l^\pm \rightarrow C l^\pm l^\mp$, where A, B, C are NP particles, e.g. in the MSSM $\tilde{\chi}_2^0, \tilde{l}, \tilde{\chi}_1^0$. Here the dilepton invariant mass distribution *rises* up to its endpoint and is therefore robust in the presence of diffuse backgrounds.

decay to the specified endstate, invariant masses constructed from the final jet and lepton momenta attain endpoint values for certain kinematic configurations only. At threshold production, in particular, one special configuration will simultaneously maximize several invariant masses; collecting a large number of threshold decays, a 2-d or 3-d scatter plot of these invariants would exhibit a clustering around this ‘threshold point.’ Yet threshold production is clearly only an infinitesimal possibility and superimposing events for ‘above-threshold’ production ($m_{\mathbb{X}} > m_A + m_B$) would probably hide the threshold point (hereafter called a ‘hidden threshold’). Contrary to this intuition, however, we find that, for some invariant mass combinations, the hidden threshold is highly visible, being in fact fortified by above-threshold events. This allows us to directly measure³ values of threshold invariant mass endpoints which, as usual, can be used to constrain NP masses. Moreover, backgrounds should not be a problem since these have different invariant-mass correlations.

The precise mechanism of this Hidden Threshold (HT) technique is best illustrated by example, which in this work we take to be

$$\mathbb{X} \rightarrow \tilde{\chi}_i^0 \tilde{\chi}_j^0 (\rightarrow \tilde{\ell}^\pm \ell^\mp \rightarrow \ell^+ \ell^- \tilde{\chi}_1^0) \quad (i, j = 2, 3, 4) \quad (1)$$

i.e. neutralino pair-production (via any parent channel) and decay to leptons ($\ell = e, \mu$). Section 2 explains the basic HT theory in this case, followed in Section 3 by application to Monte Carlo (MC) generated data simulating a low-luminosity ($10 - 30 \text{ fb}^{-1}$) run at the LHC for two different MSSM parameter points: one with on-shell slepton decays, and another with off-shell decays. Finally, Section 4 summarizes these results and suggests many avenues for further application.

2 The Hidden Threshold Technique

2.1 Base Case: Pure Higgs Decay

Let us explain the HT technique in three steps, the first of which will be the case where \mathbb{X} in (1) is a single particle which therefore has a fixed mass, say a heavy Higgs boson (H or A , hereafter designated ‘Higgs’):

$$pp \rightarrow H/A \rightarrow \tilde{\chi}_i^0 \tilde{\chi}_j^0 \rightarrow \tilde{e}^\pm e^\mp \tilde{\mu}^\pm \mu^\mp \rightarrow e^+ e^- \mu^+ \mu^- \tilde{\chi}_1^0 \tilde{\chi}_1^0 \quad (2)$$

For now, let us take the intermediate sleptons to be on-shell (see Sec. 3.2 below for the case of off-shell decays). We studied this decay chain in [8], and for the convenience of the reader we briefly recapitulate. From the four observable final lepton momenta in (2), one can define seven independent invariant mass combinations. These we

³There is also no need to ‘fit’ these endpoints, as we will see later.

defined as follows (leptons labelled as 1, 1', 2, 2', see Fig. 1):

$$M_{4l}^2 \equiv (p_1 + p_{1'} + p_2 + p_{2'})^2 \quad (3)$$

$$\begin{aligned} \overline{M}_{2l2l}^4 &\equiv \{(p_1 + p_{1'} - p_2 - p_{2'})^4 + (p_1 + p_{2'} - p_2 - p_{1'})^4 \\ &\quad + (p_1 + p_2 - p_{1'} - p_{2'})^4\}/3 \end{aligned} \quad (4)$$

$$\begin{aligned} \overline{M}_{l3l}^4 &\equiv \{(p_1 + p_{1'} + p_2 - p_{2'})^4 + (p_1 + p_{1'} + p_{2'} - p_2)^4 \\ &\quad + (p_1 + p_2 + p_{2'} - p_{1'})^4 + (p_2 + p_{2'} + p_{1'} - p_1)^4\}/4 \end{aligned} \quad (5)$$

$$\begin{aligned} \overline{M}_{l2l}^4 &\equiv \{(p_1 + p_{1'} - p_2)^4 + (p_1 + p_{1'} - p_{2'})^4 + (p_1 + p_2 - p_{2'})^4 \\ &\quad + (p_2 + p_{2'} - p_{1'})^4 + (p_1 - p_{1'} + p_2)^4 + (p_1 - p_{1'} + p_{2'})^4 \\ &\quad + (p_1 - p_2 + p_{2'})^4 + (p_2 - p_{2'} + p_{1'})^4 + (p_{1'} + p_2 - p_1)^4 \\ &\quad + (p_{1'} + p_{2'} - p_1)^4 + (p_2 + p_{2'} - p_1)^4 + (p_{2'} + p_{1'} - p_2)^4\}/12 \end{aligned} \quad (6)$$

$$\begin{aligned} \overline{M}_{3l}^4 &\equiv \{(p_1 + p_{1'} + p_2)^4 + (p_1 + p_{1'} + p_{2'})^4 \\ &\quad + (p_1 + p_2 + p_{2'})^4 + (p_2 + p_{2'} + p_{1'})^4\}/4 \end{aligned} \quad (7)$$

$$\begin{aligned} \overline{M}_{ll}^4 &\equiv \{(p_1 + p_{1'})^4 + (p_1 + p_{2'})^4 + (p_1 + p_2)^4 \\ &\quad + (p_2 + p_{2'})^4 + (p_2 + p_{1'})^4 + (p_{1'} + p_{2'})^4\}/6 \end{aligned} \quad (8)$$

$$a_4 \equiv p_1^\mu p_{1'}^\nu p_2^\rho p_{2'}^\sigma \epsilon_{\mu\nu\rho\sigma} \quad (9)$$

Adding the usual dilepton invariants M_{ee} and $M_{\mu\mu}$ to this list, we studied all distributions (1-d histograms) and derived analytic formulae for their associated endpoints (see [8] for exact expressions, too lengthy to reproduce here). In MC simulations of LHC data (assuming a luminosity of $L = 300 \text{ fb}^{-1}$) at several MSSM points where both neutralinos and both sleptons were degenerate, endpoint precisions were not high enough to give better than 30% determination of the unknown masses m_H , $m_{\tilde{l}}$, $m_{\tilde{\chi}_j^0}$, and $m_{\tilde{\chi}_1^0}$ (hereafter we abbreviate $m_s \equiv m_{\tilde{l}}$, $m_i \equiv m_{\tilde{\chi}_i^0}$). This rather unexpectedly poor resolution from a seemingly over-constrained system (seven⁴ constraints on four unknowns) owes to the highly non-linear form of the endpoint formulae, which generically yield a discrete set of solutions — adding in smearing and detector effects melds this discrete set into the large continuous range quoted. However, if one of the masses were already known to 5% accuracy, the degeneracy of the solutions breaks and the other three masses are likewise well-determined. Though our choice of invariants in (3)-(9) is somewhat more complicated (yet more systematic) than is customary, the above is nonetheless a standard illustration of the usual invariant mass endpoint method.

2.2 Threshold Higgs

Next, we consider what happens if the two neutralinos in (2) are produced at threshold⁵, that is when $m_H = m_i + m_j$ exactly. Now, it turns out, five of the invariants

⁴We did not derive an endpoint formula for a_4 ; however, we could numerically see it did not make a difference.

⁵This situation was far from realized in [8], where the Higgs mass was set fairly high, $m_H \sim 400 - 600 \text{ GeV}$.

defined above (M_{4l} , \overline{M}_{2l2l} , \overline{M}_{l2l} , \overline{M}_{3l} , and \overline{M}_{ll}), in addition to M_{ee} and $M_{\mu\mu}$, are simultaneously maximal when the kinematic configuration shown in Fig. 1 is realized.

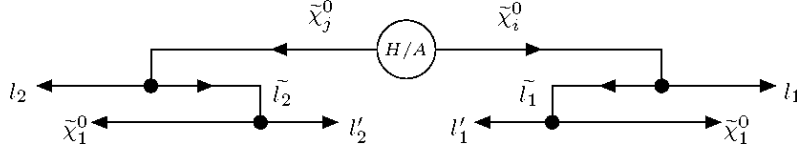


Figure 1: Kinematic configuration which simultaneously maximizes M_{4l} , \overline{M}_{2l2l} , \overline{M}_{l2l} , \overline{M}_{3l} , \overline{M}_{ll} , and $(M_{ee} \times M_{\mu\mu})$ at threshold ($m_H = m_i + m_j$).

With a suitably large sample of events, we need only plot one invariant against another to get its maximal value, as shown in Figure 2. Note that the endpoints tend to lie at a fairly triangular apex, therefore well-approximated as the intersection of two tangents to the ‘correlation shape’. Moreover, this correlation retains its shape in the presence of backgrounds, since these latter do not have the correct correlations among the various invariants and would tend to form a diffuse halo around the more concentrated signal shape. Compared to the traditional one-dimensional histogram approach, where backgrounds are harder to subtract and endpoints must be fit with a more arbitrary function, the reader can begin to appreciate that a technique using correlated invariants is much more powerful. Though this case of threshold production is not particularly likely in the MSSM, it prepares us for the next step.

2.3 Continuous Superposition of Higgses

Consider now the case where not a single Higgs decays in (2), but rather a continuum of Higgs with masses in the range $m_i + m_j \leq m_H < \infty$. Fig. 3 shows what to expect for several strategically-chosen⁶ choices of invariants: threshold decays are plotted in gray, while all above-threshold decays are plotted in black⁷. The key observation to make here is that the threshold points P(Q) in Fig. 3a(b) are not at all obscured when above-threshold events are superimposed; in fact, these latter serve to graphically reinforce the threshold points, located on the envelope of the collective shape.

It should be clear, however, that without our color-coding in Fig. 3(a,b), it is not possible to tell the exact position of P and Q⁸. Nevertheless, P and Q share a tight relationship: namely, they must uniquely identify the three endpoints M_{4l}^{max} , \overline{M}_{3l}^{max} , and $(M_{ee}^{max}) \times (M_{\mu\mu}^{max})$, this last of which is obtainable from a wedgebox plot [10], i.e. a plot of M_{ee} vs. $M_{\mu\mu}$. We can therefore find the precise locations of P and Q

⁶For the specific decay topology (1), it turns out that only certain correlations between invariants are easily analyzed, these being M_{4l} vs. $\overline{M}_{3l}M_{ee}M_{\mu\mu}$, \overline{M}_{3l} vs. $M_{4l}M_{ee}M_{\mu\mu}$, \overline{M}_{3l} vs. $M_{4l}\overline{M}_{2l2l}$, \overline{M}_{3l} vs. $M_{4l}\overline{M}_{l2l}$, and \overline{M}_{ll} vs. $\overline{M}_{2l2l}\overline{M}_{l2l}$.

⁷Threshold decays obviously contribute only infinitesimally to the total shape, but for the sake of seeing how these are distributed compared to above-threshold decays, we plotted 10^3 of these on top of 10^6 above-threshold events.

⁸There is a sort of kink near P and Q, but this turns out to be related to $M_{\ell+\ell-}^{max}$ only.

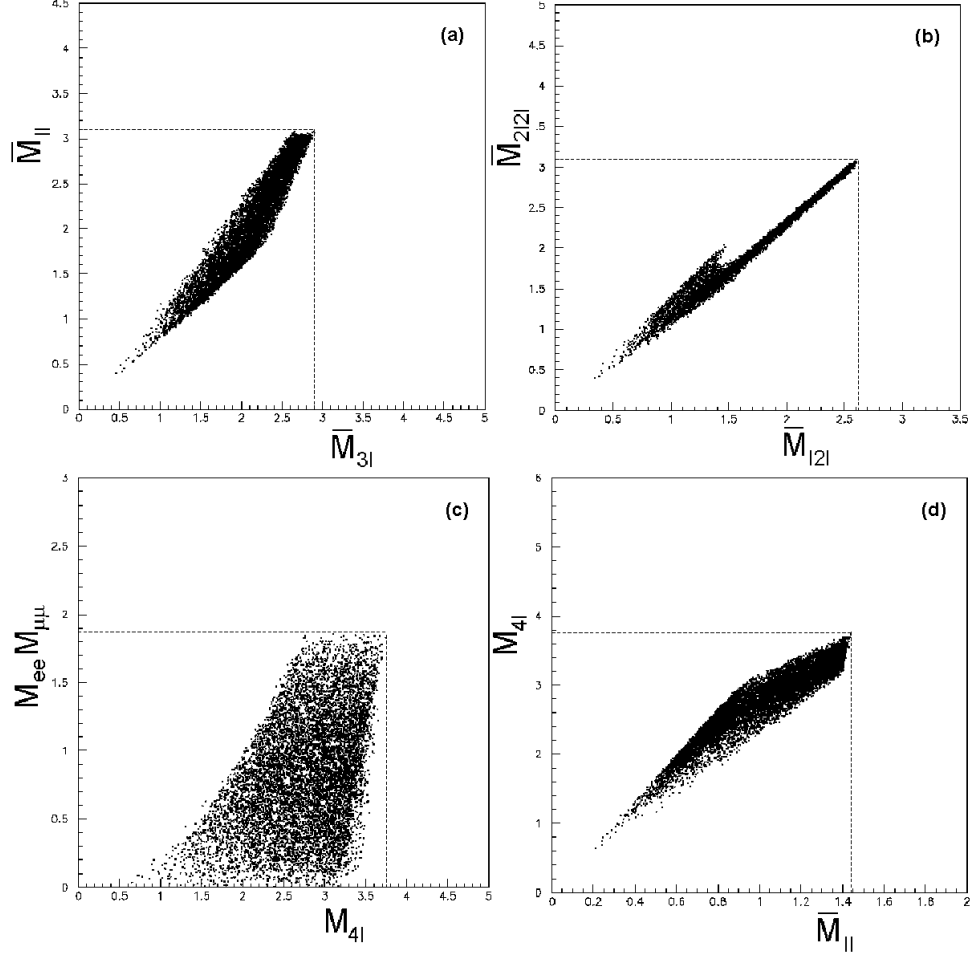


Figure 2: Various correlations of four-lepton invariant masses at threshold ($m_H = m_i + m_j$). This simulation is purely from relativistic kinematics with $(m_1, m_i, m_j, m_s) = (1, 3, 4, 1.1)$ (units arbitrary). Dashed lines mark the maximum value of each invariant.

with a graphical device: superimpose a plot of M_{4l} vs. $\overline{M}_{3l} \frac{(M_{ee}) \times (M_{\mu\mu})}{(M_{ee}^{max}) \times (M_{\mu\mu}^{max})}$ with one of $M_{4l} \frac{(M_{ee}) \times (M_{\mu\mu})}{(M_{ee}^{max}) \times (M_{\mu\mu}^{max})}$ vs. \overline{M}_{3l} (i.e. superimpose Fig. 3a and Fig. 3b with swapped and rescaled axes). This gives rise to a characteristic 'cat-eye' shape (Figure 3c), where the upper corner of the eye pinpoints the correct threshold extrema of M_{4l} and \overline{M}_{3l} .

There is another very useful correlation here, namely \overline{M}_{3l} vs. $M_{4l} \overline{M}_{2l2l}$ (see previous footnote for alternatives). Analogous to the situation in Fig. 3a and Fig. 3b, threshold values of \overline{M}_{3l}^{max} and $M_{4l}^{max} \overline{M}_{2l2l}^{max}$ for this $\mathbb{X} \rightarrow \tilde{\chi}_i^0 \tilde{\chi}_j^0$ decay again lie on the envelope of the correlation shape at point 'X' in Fig. 3d; what is more interesting, every point on the envelope *above* X (say, 'Y' in Fig. 3d) corresponds to another set of $\overline{M}_{3l}^{max'}$ and $M_{4l}^{max'} \overline{M}_{2l2l}^{max'}$ for a decay $\mathbb{X} \rightarrow \zeta \xi$, where ζ and ξ are some hypothetical set of heavier particles ($m_{\zeta, \xi} > m_{i, j}$) which follow the same decay chain through an on-shell slepton to leptons and the LSP. In other words, if ζ and ξ really were produced, they would have decay kinematics leading precisely to the endpoints identified

at Y (we will call this a ‘pseudo-threshold’). Every such pseudo-threshold therefore yields a set of endpoints $\overline{M}_{3l}^{max'}$ and $M_{4l}^{max'} \overline{M}_{2l2l}^{max'}$ which can be used to constrain m_1 , m_s , and m_ζ (where without loss of generality we can take $\zeta = \xi$), this latter being merely an auxiliary parameter at each such point. What we are effectively saying here is that the shape of the envelope above X depends on m_1 and m_s only, and sufficiently precise measurement of this envelope can constrain these parameters.

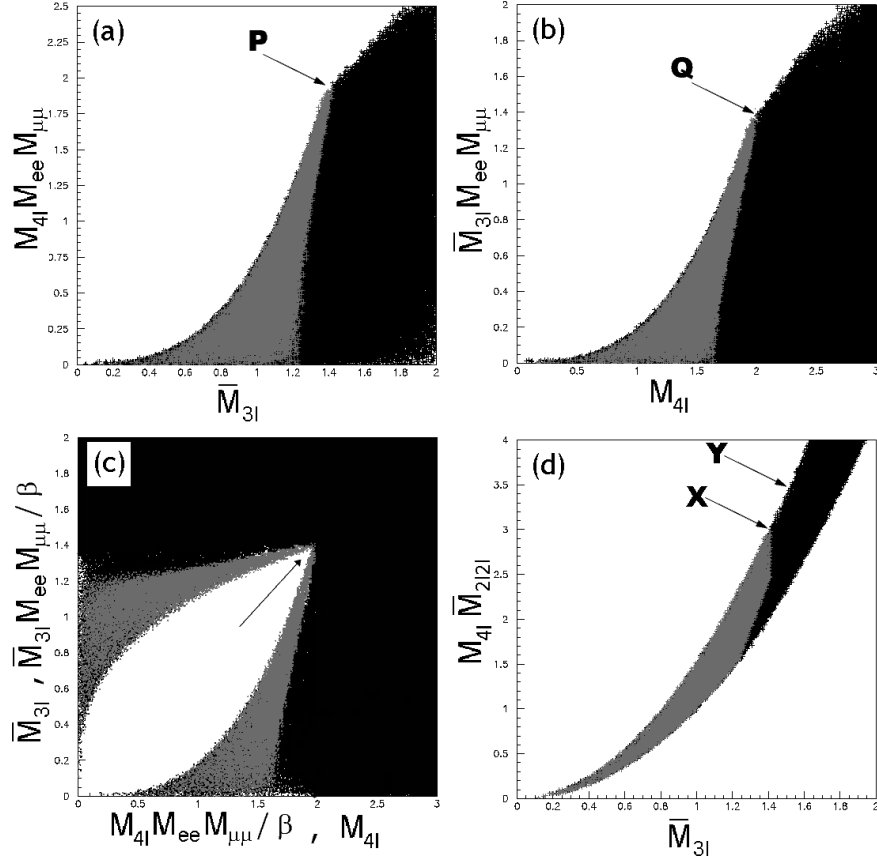


Figure 3: *Correlations of various invariant masses in a superposition of many Higgs decays (2) with a continuum of masses in the range $m_i + m_j \leq m_H < \infty$ (again from relativistic kinematics only, with $(m_1, m_i = m_j, m_s) = (1, 2, 1.5)$ in arbitrary units). Points P and Q in (a) and (b) identify threshold endpoints; these can be found precisely with a ‘cat-eye’ plot in (c), where we have abbreviated $\beta \equiv (M_{ee}^{max}) \times (M_{\mu\mu}^{max})$. In (d) we show another useful correlation of invariants which not only gives threshold endpoints at X, but also ‘pseudo-threshold’ endpoints at any point Y higher up on the envelope.*

Now there is really no difference between this situation with a continuously-massed Higgs and that of the decay (1), or more specifically

$$\mathbb{X} \rightarrow \mathbb{X}' + \tilde{\chi}_i^0 (\rightarrow \tilde{e}^\pm e^\mp \rightarrow e^+ e^- \tilde{\chi}_1^0) \tilde{\chi}_j^0 (\rightarrow \tilde{\mu}^\pm \mu^\mp \rightarrow \mu^+ \mu^- \tilde{\chi}_1^0) \quad (10)$$

where \mathbb{X} could be pp , $\tilde{q}\tilde{q}'$, $\tilde{q}\tilde{g}$, $\tilde{g}\tilde{g}$, $\tilde{\chi}_2^\pm \tilde{\chi}_2^\mp$ etc., or any two⁹ SUSY particles with a continuous center of mass energy greater than or equal to $m_i + m_j$, while \mathbb{X}' are any

⁹The present work assumes R-parity is exact, though the general technique does not require this.

collection of particles, e.g. hadronic jets, that do not confuse the 4-lepton signal. As long as the neutralino-pair subchains are intact, the mother chain is irrelevant. Note also we do not require the lightest neutralino to be stable, as long as its decay products do not include leptons. As we shall see in the next section this technique works very well in MC simulations with a minimal requirement of four isolated leptons plus missing energy.

3 Examples of Applications

In this section we demonstrate the robustness of our technique at two different MSSM parameter points with varying decay topologies. Our MC setup uses HERWIG 6.5 and private codes as in our previous publications [8, 9, 10] and the reader is referred to these for details.

We generate events

$$pp \rightarrow \{\tilde{q}, \tilde{g}, \tilde{\chi}_{1,2}^{\pm}, \tilde{\chi}_{1,2,3,4}^0\} + \{\tilde{q}, \tilde{g}, \tilde{\chi}_{1,2}^{\pm}, \tilde{\chi}_{1,2,3,4}^0\} \quad (11)$$

for $10-30 \text{ fb}^{-1}$ (a low-luminosity year at the LHC) and only pass those which decay to a hard and isolated e^+e^- and $\mu^+\mu^-$ pair with sufficient missing energy ($E_T > 20 \text{ GeV}$). This eliminates SM backgrounds aside from $pp \rightarrow Z^*Z$, though this can be modeled and subtracted (by a Z-veto if necessary, which happens to work perfectly at the parameter points we will consider). SUSY backgrounds fall into two categories: those which produce exactly four leptons and those which produce more than this (presumably losing some to isolation cuts, detector effects, etc.). The first category includes slepton or chargino ‘3+1’ decays such as $\tilde{\chi}_2^{\pm} (\rightarrow l^{\pm} l'^{\pm} l''^{\mp} \nu \nu' \bar{\nu}') \tilde{\chi}_1^0$ $\tilde{\chi}_1^{\mp} (\rightarrow l''^{\mp} \nu'' \tilde{\chi}_1^0)$ where one decay goes to three leptons and the other to one. These could always be substantially reduced via flavor subtraction, but this is not necessary since they have totally different kinematics from a ‘2+2’ decay (i.e. (10)) and should not obscure the envelopes in plots such as Fig. 3. Moreover, such decays would exhibit their own characteristic correlation shapes in addition to the trilepton invariant mass edge. In the worst case, then, four-lepton SUSY backgrounds should be considered an ‘enriched signal.’ The second category of SUSY backgrounds includes events such as $\tilde{\tau}\tilde{\tau}$ where each stau decays $\tilde{\tau} \rightarrow \tau \tilde{\chi}_2^0 \rightarrow l^{\pm} l'^{\pm} l''^{\mp} \nu \nu' \tilde{\chi}_1^0$ and two of the total of six leptons are somehow lost. Yet such events, if not made utterly small by leptonic branching fractions, would introduce a more-or-less diffuse halo in our correlation plots, and in particular should not confuse the identification of threshold points.

3.1 On-Shell Box

The most basic illustration of the HT technique for the decay (10) is when only one particular (i, j) -combination has a significant branching ratio; if, in addition, $i = j$, threshold endpoint formulae simplify dramatically, e.g.

$$M_{4l}^{max} = \frac{m_j^2(2m_j^2 m_s^2 - m_1^2) - m_s^4}{m_j m_s^2} \quad (12)$$

Table 1: *Relevant masses at the On-Shell Point and Off-Shell Point (all masses in GeV).*

	$\tilde{\chi}_1^0$	$\tilde{\chi}_2^0$	$\tilde{\chi}_3^0$	$\tilde{\chi}_4^0$	$\tilde{e}_R, \tilde{\mu}_R$	$\tilde{\chi}_1^\pm$	$\tilde{\chi}_2^\pm$
On-Shell	117.1	197.5	257.2	317.7	134.7	193.3	317.0
Off-Shell	79.6	131.5	160.6	249.5	148.0	115.6	249.0

A $\tilde{\chi}_2^0\tilde{\chi}_2^0$ pair, for example, is often the chief product of colored cascades at mSUGRA points such as SPS1a [3]. Though we have checked our technique works at SPS1a, we choose another point which has higher rates and therefore better demonstrates the agreement with theory presented in the last section:

On-Shell Point

$$\begin{aligned}
\mu &= 250 \text{ GeV} & M_2 &= 250 \text{ GeV} & M_1 &= 125 \text{ GeV} \\
\tan\beta &= 10 & M_{\tilde{\tau},(\tilde{e},\tilde{\mu})_L} &= 250 \text{ GeV} & M_{(\tilde{e},\tilde{\mu})_R} &= 130 \text{ GeV} \\
m_H &= 700 \text{ GeV} & M_{\tilde{q}} &\approx 400 \text{ GeV} & M_{\tilde{g}} &\approx 500 \text{ GeV}
\end{aligned}$$

Here we have raised the left-handed slepton and stau soft mass inputs above those of the right-handed selectron and smuon (note the physical masses differ slightly from these, see Table 1) to suppress sneutrino exchange and stau modes which may reduce the magnitude of (but not character of) the signal. The heavy Higgs mass is set rather high to remove it from the analysis, but setting it lower would in fact be beneficial since Higgs contribute to the signal process $\mathbb{X} \rightarrow \tilde{\chi}_i^0\tilde{\chi}_j^0$.

With a luminosity of 30 fb^{-1} the wedgebox plot in Figure 4a is a very dense and symmetric box structure, which strongly suggests degenerate neutralinos decaying via degenerate sleptons¹⁰. Since the dilepton mass distribution (Figure 4b) is quite triangular, we could also guess that the sleptons are on-shell — in the next subsection we will show how to establish this quantitatively.

Thus, being certain of having a fairly homogenous sample of $\mathbb{X} \rightarrow \tilde{\chi}_2^0\tilde{\chi}_2^0$ decays, where each neutralino decays as $\tilde{\chi}_2^0 \rightarrow \tilde{\ell}^\pm \ell^\mp \rightarrow \ell^+ \ell^- \tilde{\chi}_2^0$ with a dilepton edge $M_{\ell^+\ell^-} \sim 75 \text{ GeV}$, we can directly proceed to construct a cat-eye plot in Fig. 4c to determine threshold values of M_{4l}^{max} and \overline{M}_{3l}^{max} . Note that even at this low luminosity, the threshold point (marked as a large black dot in Fig. 4c) can be located to a few GeV precision: we measure $(M_{4l}^{max}, \overline{M}_{3l}^{max}) = (150 \pm 5, 107 \pm 5) \text{ GeV}$. This is quite close to the expected values of (153.9, 112.4) GeV found by plugging in masses from Table 1 into formulae in the Appendix. The HT method is working.

Having determined \overline{M}_{3l}^{max} from the cat-eye plot, we proceed to measure a number of pseudo-threshold points in a plot of \overline{M}_{3l} vs. $M_{4l}\overline{M}_{2l2l}$ for $\overline{M}_{3l} > \overline{M}_{3l}^{max}$ (see Fig. 4d). Table 2 compares some of our measurements to expected values over a liberal range of \overline{M}_{3l} , where the reader can verify good agreement. Using a large number n of

¹⁰Strictly speaking this could also be a chargino decaying via a sneutrino, i.e. $\tilde{\chi}_2^\pm \rightarrow l^\pm \tilde{\nu} \rightarrow l^\pm l^\mp \tilde{\chi}_1^\pm$. Other signs such as the number of 6-lepton events (after $\tilde{\chi}_1^\pm \rightarrow l^\pm \nu \tilde{\chi}_1^0$) might resolve this ambiguity.

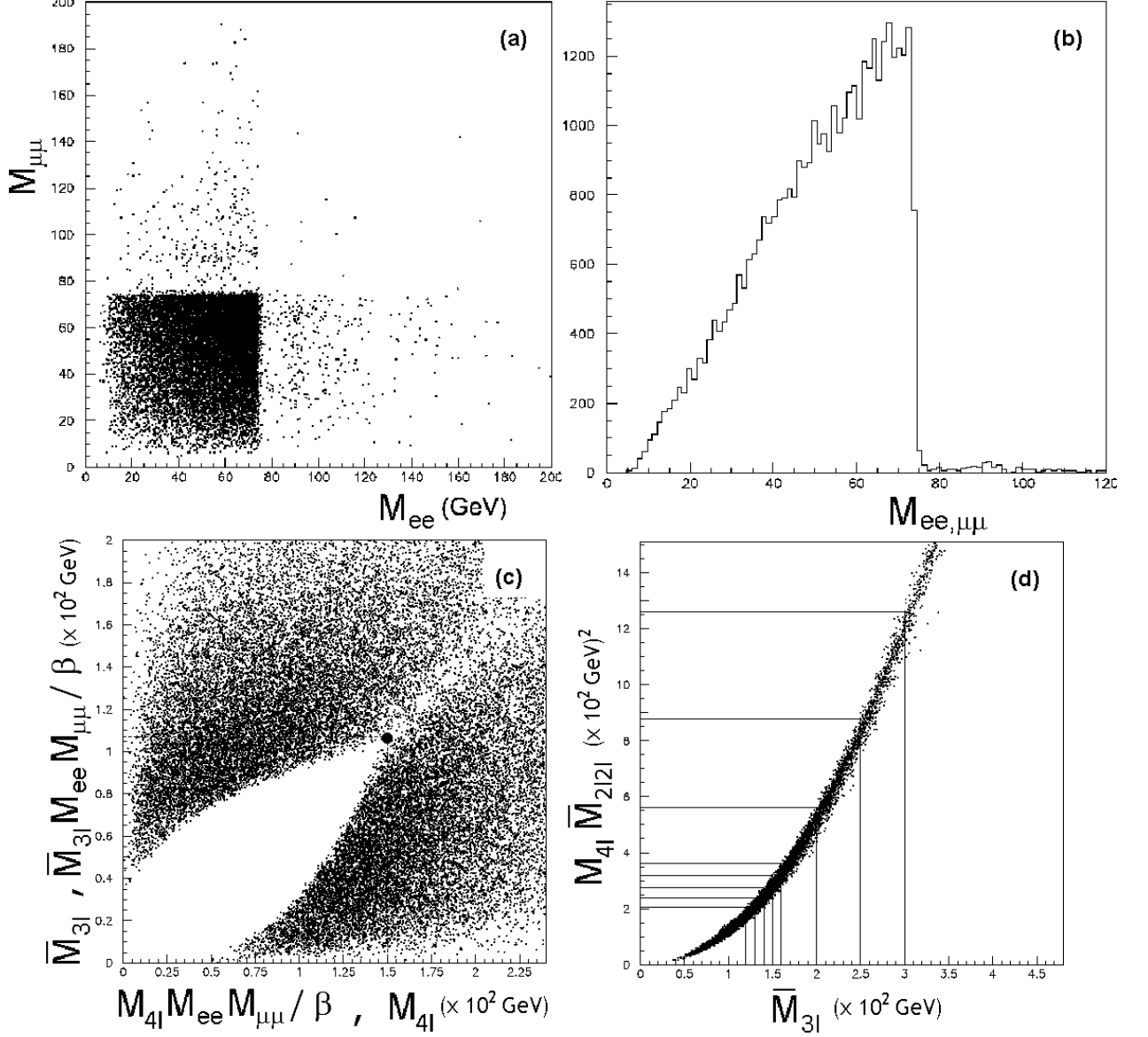


Figure 4: Various plots for the On-Shell Point with 30 fb^{-1} luminosity. The wedgebox plot (a) is mostly box-like with a triangular dilepton mass distribution (b) typifying an on-shell decay. The threshold values of M_{4l} and \bar{M}_{3l} for the $\tilde{\chi}_2^0 \tilde{\chi}_2^0$ resonance ($\beta = (75 \text{ GeV})^2$) in the cat-eye plot (c) are easily identified at the ‘corner of the eye’ (the black dot). We proceed to measure several points along the envelope of the shape in (d) for $\bar{M}_{3l} > \bar{M}_{3l}^{max}$; these can be used to constrain the slepton and LSP masses.

measurements (say $n = 30$) we search $(m_1, m_s, m_{\zeta_1}, m_{\zeta_2}, \dots, m_{\zeta_n})$ -space for the best fit to the corresponding $(\bar{M}_{3l}^{max}, M_{4l}^{max} \bar{M}_{2l^2}^{max})_{i=1..n}$, using analytical expressions in the Appendix. We find $m_1 = 116 \pm 10 \text{ GeV}$ with the slepton mass shifted by a near constant, $m_s = (m_1 + 17) \pm 2 \text{ GeV}$. From these and the dilepton edge $M_{\ell+\ell^-} = 75 \pm 1 \text{ GeV}$, we can likewise determine $m_2 = 210 \pm 12 \text{ GeV}$. With a higher luminosity sample (say, 300 fb^{-1}) error-bars could certainly be reduced by a factor of several;

Table 2: *Measurements of $M_{4l}\overline{M}_{2l2l}$ for various \overline{M}_{3l} at the On-Shell Point (viz. Fig. 4d) and comparison to theoretical values (boldface) assuming these correspond to pseudo-thresholds, i.e. plugging slepton and LSP masses from Table 1 and m_ζ (in place of m_j) into formulae in the Appendix (all masses in GeV).*

\overline{M}_{3l}	$M_{4l}\overline{M}_{2l2l}$	Theory	m_ζ
120	205 ± 1	205.6	203.2
130	239 ± 1	240.3	211.0
140	275 ± 2	278.0	219.0
150	318 ± 2	318.0	227.0
160	363 ± 2	360.9	235.2
200	560 ± 5	559.9	269.0
250	875 ± 5	868.0	313.0
300	1260 ± 5	1250.6	595.5

in this case the masses (m_1, m_s, m_2) can ultimately be found to about 2% accuracy.

3.2 Off-Shell Box

Decays through off-shell sleptons are simpler for two reasons. First, mathematically speaking, invariant mass edges do not depend on slepton masses; in the case of a box topology these can therefore only depend on m_1 and m_j . Since the dilepton mass edge is equal to the difference of these, $(m_j - m_1)$, we only need one other function of these masses to determine them.

Secondly, the physical degrees of freedom are easier to analyze: for threshold decays in particular, each neutralino $\tilde{\chi}_j^0$ is at rest in the center of mass frame and leptonic invariants are maximized/minimized when the same flavor leptons are emitted antiparallel/parallel. The product $(M_{ee}) \times (M_{\mu\mu})$ is therefore maximal when the electron(muon) is antiparallel to the positron(anti-muon), and is equal to $(m_j - m_1)^2$. For this kinematical configuration, however, all the other invariants M_{4l} , \overline{M}_{2l2l} , \overline{M}_{l2l} , \overline{M}_{3l} , and \overline{M}_{ll} are equal(up to a constant factor) to $(m_j - m_1)$ and therefore do not provide independent information.

The trick is to consider configurations where the electron and positron are antiparallel while the muon and anti-muon are parallel (or vice versa). In this case M_{ee} or $M_{\mu\mu}$ is maximal and the other invariants (excepting \overline{M}_{l2l}) unconditionally attain *minima* when the e^+e^- pair is emitted at right angles to the $\mu^+\mu^-$ pair:

$$\overline{M}_{4l,2l2l,3l,ll}^{min} = (m_j - m_1) \left(\frac{\alpha + \beta \frac{m_1}{m_j} + \gamma \frac{m_1^2}{m_j^2}}{\xi} \right)^{\frac{1}{4}} \quad (13)$$

for specific values of the parameters α , β , γ , and ξ listed in Table 3. Thus, any one of these in conjunction with the dilepton mass edge uniquely determines m_j and m_1 . Geometrically, these endpoints are found at the intersection of the line

$M_{l+l-} = (m_j - m_1)$ with the near edges of the correlation shapes on a plot of M_{l+l-} versus M_{4l} , \overline{M}_{2l2l} , \overline{M}_{3l} , or \overline{M}_{ll} . These intersections can be found with high precision and then checked against each other for consistency.

To see the efficacy of this method, consider the following parameter point (see Table 1 again for the physical spectrum):

Off-Shell Point

$$\begin{aligned} \mu &= 150 \text{ GeV} & M_2 &= 200 \text{ GeV} & M_1 &= 100 \text{ GeV} \\ \tan \beta &= 10 & M_{\tilde{\tau},(\tilde{e},\tilde{\mu})_L} &= 300 \text{ GeV} & M_{(\tilde{e},\tilde{\mu})_R} &= 135 \text{ GeV} \\ m_H &= 700 \text{ GeV} & M_{\tilde{g}} &\approx 300 \text{ GeV} & M_{\tilde{q}} &\approx 350 \text{ GeV} \end{aligned}$$

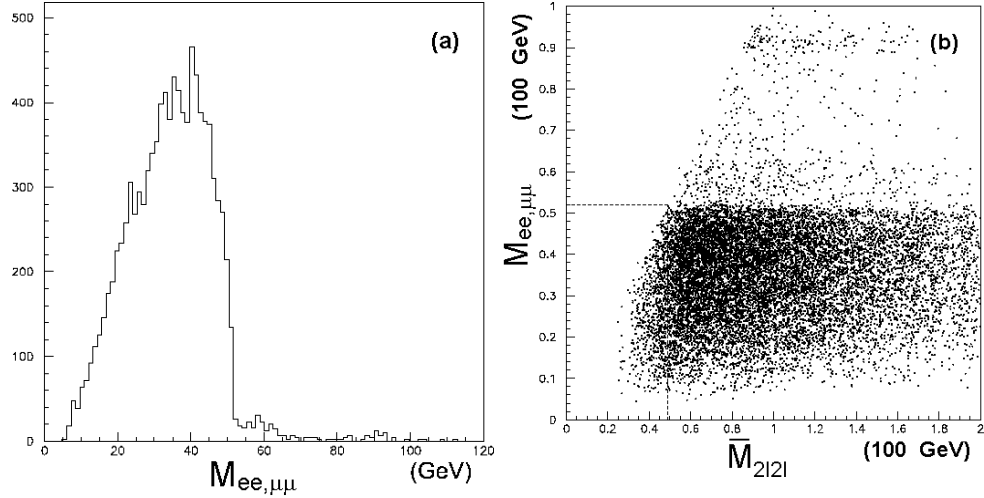


Figure 5: *MC Simulation at the Off-Shell Point for 10 fb^{-1} luminosity. The dilepton invariant mass distribution in (a) indicates a maximum of about $M_{l+l-}^{max} \sim 52 \text{ GeV}$. In (b) we show where this maximum is coincident with the minimum value of \overline{M}_{2l2l} at the dotted line, which is to be matched against expression (13). Corresponding plots for the other invariants look very similar.*

Though the 10 fb^{-1} dilepton mass distribution in Fig. 5a looks very similar to that of the On-Shell Point, the dilepton edge at $M_{l+l-}^{max} \sim 52 \text{ GeV}$ is in fact due to three-body decays via off-shell sleptons. We might guess this from the vaguely less-than-triangular shape, but now we have a better way. We simply plot M_{l+l-} versus each of the invariants M_{4l} , \overline{M}_{2l2l} , \overline{M}_{3l} , and \overline{M}_{ll} (e.g. Fig. 5(b)) and match against the formulae in (13). Table 3 shows that these give mutually consistent values of m_1 and m_j , which at high luminosity may be determined to several percent or so. Had we constructed the same plots at our On-Shell Point, we would have obtained a set of endpoints which give inconsistent, even nonsensical values for $m_{1,j}$ (e.g. negative LSP mass!). Though the dilepton distributions of Fig. 4b and Fig. 5a give qualitative hints of whether sleptons are on- or off-shell, here we seem to have the

Table 3: *Offshell Decay Parameters in (13) and Fits to MC data at the Off-Shell Point for the LSP mass (m_1), assuming the dilepton edges are exact and 0.2 GeV precision on other endpoints. Also shown are attempted fits to data at the On-Shell Point which, even with larger(± 1 GeV) errors, give self-inconsistent results.*

Invariant	α	β	γ	ξ	LSP(Off)	LSP(On)
M_{4l}^{min}	4	4	1	1	85 ± 5	22 ± 5
$\overline{M}_{2l2l}^{min}$	2	0	1	3	85 ± 11	172 ± 78
\overline{M}_{3l}^{min}	11	10	3	8	84 ± 6	1 ± 5
\overline{M}_l^{min}	3	2	1	48	86 ± 15	-8 ± 10

first definitively *quantitative* method of determining this which succeeds even with modest(several GeV) endpoint precision.

4 Conclusions

Let us now summarize the HT technique and how we applied it in this work:

1. DEFINE the decay chain $\mathbb{X} \rightarrow \mathbb{X}' + ABC... \rightarrow n_j \text{ jets} + n_l \text{ leptons}$, where \mathbb{X} is anything and \mathbb{X}' is exclusive of jets and leptons. *In our case this was $\mathbb{X} \rightarrow \tilde{\chi}_i^0 \tilde{\chi}_j^0$ where each neutralino then decayed via a slepton to a pair of leptons and the LSP.*
2. DERIVE analytic expressions for all jet and lepton invariant mass endpoints as functions of NP masses, and find kinematic configurations for which two or more of these are extremal at threshold production. *In our case of four leptons($n_l = 4$), there are in principle 7 independent invariants; of these, we found $(M_{ee}) \times (M_{\mu\mu})$, M_{4l} , \overline{M}_{2l2l} , \overline{M}_{l2l} , \overline{M}_{3l} , and \overline{M}_l were simultaneously maximal for on-shell decays, whereas for off-shell decays $M_{ee}(M_{\mu\mu})$ was maximal(minimal) where M_{4l} , \overline{M}_{2l2l} , \overline{M}_{3l} , and \overline{M}_l were minimal.*
3. DISPLAY correlations of the above invariants in a scatterplot which makes their threshold endpoints visually obvious. Use these to solve for NP masses. *For off-shell slepton decays it sufficed to plot each invariant versus M_{l+l-} and note the intersection with the line $M_{l+l-} = M_{l+l-}^{max}$. For on-shell decays we found it useful to make a cat-eye plot to find the threshold value of \overline{M}_{3l}^{max} , followed by measuring several pseudo-thresholds in a plot of \overline{M}_{3l} vs. $M_{4l}\overline{M}_{2l2l}$. Matching to analytical expressions constrains (m_1, m_2, m_s) to within a few percent of their nominal values.*

Let us add a few remarks on these three steps. The first step depends of course on the specific NP model under consideration, but once a decay chain has been selected, deriving analytical formulae for endpoints in the second step is not difficult: the

sought-after kinematic configuration is usually where each jet or lepton is emitted at a polar angle of $\theta = 0$ or $\theta = \pi$ or perhaps $\theta = \pi/2$ (for minima) in the frame of the decaying parent particle, backwards Lorentz-boosting to the center-of-mass frame (see Appendix of [8] for an example). Choosing which invariants to plot in the third step is a matter of trial-and-error — kinematic simulation (as in Fig. 2 and Fig. 3) can be used to see which correlations have a visible threshold point when above-threshold decays are superimposed.

To demonstrate the general applicability of this technique to NP, we present below a partial spectrum of examples. Each example in itself entails numerous variations (e.g. on-shell intermediate states could likewise be taken off-shell):

- Neutralino Decay via higgs: $\tilde{\chi}_2^0 \tilde{\chi}_2^0 (\rightarrow \tilde{\chi}_1^0 h (\rightarrow bb))$. This $n_j = 4$ decay is a potential competitor to the sleptonic modes considered in this paper.
- Sneutrino Pair Production: $\tilde{\nu} \tilde{\nu} (\rightarrow l^\pm \tilde{\chi}_1^\mp (\rightarrow \tilde{\chi}_1^0 W^- (\rightarrow l'^\mp \nu')))$ Here $n_l = 4$ as for neutralino pair production, but with totally different kinematics: one can analogously define M_{4l} , \overline{M}_{2l2l} , \overline{M}_{l3l} , etc., though threshold extrema of these will have a different correlation.
- Chargino Pair Production: $\tilde{\chi}_2^\pm \tilde{\chi}_2^\mp (\rightarrow l^\mp \tilde{\nu} (\rightarrow l^\pm \tilde{\chi}_1^\mp (\rightarrow l^\mp \nu \tilde{\chi}_1^0)))$ This is a $n_l = 6$ case which means there are as many as 45 relativistic invariants¹¹.
- Slepton Pair Production $\tilde{l}^\pm \tilde{l}^\mp (\rightarrow l^\mp \tilde{\chi}_2^0 (\rightarrow l^\pm l^\mp \tilde{\chi}_1^0))$. This could either be $n_l = 6$ or $n_l = 4$ depending on how the other slepton decays.
- Squark Pair Production $\tilde{q} \tilde{q} (\rightarrow q \tilde{\chi}_2^0 (\rightarrow l^\pm \tilde{l}^\mp (\rightarrow l^\mp \tilde{\chi}_1^0)))$. A $n_j = 2$, $n_l = 4$ decay with 45 invariants to analyze.
- Gluino Pair Production $\tilde{g} \tilde{g} (\rightarrow q \tilde{q} (\rightarrow q \tilde{\chi}_2^0 (\rightarrow q' q' \tilde{\chi}_1^0)))$ This $n_j = 8$ decay has an astounding 588 invariants.
- Nonstandard Higgs decays $h \rightarrow XY$ (e.g. [11])
- Exotic Vectors (from, e.g. Little Higgs [12])
- Kaluza-Klein Pair Production (e.g. [13]).
- Exotica decays to top-pairs $pp \rightarrow X \rightarrow t\bar{t}$ (e.g. [14])
- Low-Scale Technicolor (e.g. $W^\pm \pi_T \rightarrow l^\pm \nu b\bar{b}$ [15]).

The hidden threshold method provides another way to see signatures of these NP models and determine any unknown masses involved. Results can be made even stronger in combination with inclusive techniques and complementary methods of mass determination (in SUSY for example, see [6, 16, 17]). We hope that research along these lines will allow an earlier discovery of NP at hadron colliders.

¹¹The number of invariants is computed as the number of pairwise contractions among the observable momenta, as well as with powers of $\epsilon^{\mu\nu\rho\sigma}$

References

- [1] Linear Collider Collaboration, “Precision measurement of a particle mass at the linear collider.” arXiv:0712.4389 [hep-ph].
- [2] H. Bachaco, I. Hinchliffe, and F. E. Paige, “Measurements of masses in SUGRA models at LHC.” Phys.Rev.**D62**:015009 (2000).
- [3] B.C. Allenbach et al., “The Snowmass points and slopes: Benchmarks for SUSY searches,” In: N. Graf (ed.), Snowmass 2001: Proc. of APS/DPF/DPB Summer Study on the Future of Particle Physics, Snowmass, Colorado, July, 2001, page 125, arXiv: 0202233 [hep-ph]. Eur. Phys. J. C **25**: 113 (2002).
- [4] B.K. Gjelsten , D.J. Miller , and P. Osland. “Measurement of the gluino mass via cascade decays for SPS 1a.” JHEP **0506**:015 (2005).
- [5] D.J. Miller, P. Osland, and A.R. Raklev, “Invariant mass distributions in cascade decays.” JHEP **0603**:034,2006.
- [6] “ATLAS Detector and Physics Performance Technical Design Report 2”, Chapter 20, CERN-LHCC-99-015,ATLAS-TDR-15, May, 1999, <http://atlas.web.cern.ch/Atlas/GROUPS/PHYSICS/TDR/access.html>
- [7] B.C. Allanach, J.P. Conlon, and C.G. Lester, “Measuring Smuon-Selectron Mass Splitting at the LHC and Patterns of Supersymmetry Breaking.” arXiv:0801.3666 [hep-ph].
- [8] P. Huang, N. Kersting, and H.H. Yang, “Extracting MSSM Masses From Heavy Higgs Decays to Four Leptons at the LHC.” Phys. Rev. **D77**, 075011 (2008). arXiv:0801.0041 [hep-ph].
- [9] G. Bian, M. Bisset, N. Kersting, Y. Liu, and X. Wang, “Wedgebox analysis of four-lepton events from neutralino pair production at the LHC.” Eur.Phys.J.**C53**:429-446 (2008).
- [10] M. Bisset, N. Kersting, J. Li, F. Moortgat, S. Moretti, and Q.L. Xie, “Pair-produced heavy particle topologies: MSSM neutralino properties at the LHC from gluino/squark cascade decays.” Eur.Phys.J.**C45**:477-492 (2006).
- [11] S. Chang, R. Dermisek, J.F. Gunion, and N. Weiner, “Nonstandard Higgs Boson Decays.” arXiv:0801.4554 [hep-ph].
- [12] M. Schmaltz, and D. Tucker-Smith, “Little Higgs review.” Ann. Rev. Nucl. Part. Sci.**55**: 229-270 (2005).
- [13] P. Nath, Y. Yamada, and M. Yamaguchi, “Probing the Nature of Compactification with Kaluza-Klein Excitations at the Large Hadron Collider.” Phys.Lett. **B466** : 100-106 (1999).

- [14] R. Frederix and F. Maltoni, “Top pair invariant mass distribution: A Window on new physics.” arXiv:0712.2355 [hep-ph].
- [15] E. Eichten and K. Lane, “Low-scale technicolor at the Tevatron and LHC.” arXiv:0706.2339 [hep-ph].
- [16] H.-C. Cheng, J. F. Gunion, Z. Han, G. Marandella, and B. McElrath, “Mass determination in SUSY-like events with missing energy.” JHEP **0712**:076 (2007).
- [17] K. Kawagoe, M.M. Nojiri, and G. Polesello, “A New SUSY mass reconstruction method at the CERN LHC.” Phys.Rev.**D71**:035008 (2005).

Appendix

Threshold maxima for on-shell decays are readily computed via the methodology of [8]. For the case $i = j$ we just substitute $m_A = 2m_j$ in the formulae of that work for the $[+ + - -]$ configurations, obtaining the following:

$$\mathbf{M}_{41}^{\max} = \frac{m_j^2(2m_j^2m_s^2 - m_1^2) - m_s^4}{m_jm_s^2}$$

$$\overline{\mathbf{M}}_{2121}^{\max} = \frac{1}{3^{1/4}m_jm_s^2} (3m_1^8m_j^8 - 4m_1^6m_j^6m_s^2(2m_j^2 + m_s^2) - 4m_1^2m_j^2m_s^6(8m_j^6 - 12m_j^4m_s^2 + 6m_j^2m_s^4 + m_s^6) + m_s^8(16m_j^8 - 32m_j^6m_s^2 + 24m_j^4m_s^4 - 8m_j^2m_s^6 + 3m_s^8) + 6m_1^4(4m_j^8m_s^4 - 4m_j^6m_s^6 + 3m_j^4m_s^8))^{1/4}$$

$$\overline{\mathbf{M}}_{121}^{\max} = \frac{1}{6^{1/4}m_jm_s^2} (3m_1^8m_j^8 - 2m_1^6m_j^6m_s^2(5m_j^2 + m_s^2) + 6m_1^4m_j^4m_s^4(3m_j^4 - m_j^2m_s^2 + m_s^4) - 2m_1^2m_j^2m_s^6(8m_j^6 - 6m_j^4m_s^2 + 3m_j^2m_s^4 + m_s^6) + m_s^8(8m_j^8 - 16m_j^6m_s^2 + 18m_j^4m_s^4 - 10m_j^2m_s^6 + 3m_s^8))^{1/4}$$

$$\overline{\mathbf{M}}_{31}^{\max} = \frac{(m_1^4m_j^4 - 2m_1^2m_j^4m_s^2 + 2m_j^4m_s^4 - 2m_j^2m_s^6 + m_s^8)^{1/4} \sqrt{m_1^2m_j^2 - 2m_j^2m_s^2 + m_s^4}}{2^{1/4}m_jm_s^2}$$

$$\overline{\mathbf{M}}_{11}^{\max} = \frac{\sqrt{m_1^4m_j^4 - 2m_1^2m_j^4m_s^2 + 2m_j^4m_s^4 - 2m_j^2m_s^6 + m_s^8}}{24^{1/4}m_jm_s^2}$$